Molecular Orientation Depth Profiles in Organic Glasses using Polarized Resonant Soft X-ray Reflectivity

Jacob L. Thelen¹, Camille Bishop², Kushal Bagchi², Daniel F. Sunday¹, Eliot Gann¹, Subhrangsu Mukherjee¹, Lee J. Richter¹, R. Joseph Kline¹, M. D. Ediger²,*, Dean M. DeLongchamp¹,*

¹ National Institute of Standards and Technology, Gaithersburg, MD National Institute of Standards and Technology

² Department of Chemistry, University of Wisconsin-Madison, Madison, WI 53705 USA

^{*} E-mail: ediger@chem.wisc.edu; dean.delongchamp@nist.gov

Abstract

Molecular orientation anisotropy can be critical in functional organic thin films. For instance, it is known that molecular orientation can affect the performance of organic electronic devices such as light emitting diodes (OLEDs), thin film transistors (OTFTs), and photovoltaics (OPVs); however, the impact of molecular orientation on device performance tends to be obscured by complexities of the multilayer device structure, and control over molecular orientation in the organic layer(s) is often limited. Thus, techniques that can depth profile molecular orientation in thin films are sorely needed. We demonstrate that polarized resonant soft X-ray reflectivity (p-RSoXR) can extract molecular orientation depth profiles with the needed nanometer-level resolution. Leveraging developments in stable molecular glass formation using physical vapor deposition (PVD) we create molecular glass films of posaconazole, a rod-like molecule, with controlled orientation. We show that p-RSoXR is highly sensitive to thin oriented layers at the posaconazole surface, while providing quantitative molecular tilt values for the bulk film. Finally, we demonstrate that p-RSoXR can detect and characterize buried interfaces based solely on molecular orientation, providing insight into the structure of complex films that was previously unmeasurable.

Inhomogeneous vertical depth profiles are a critical aspect of nanoscale structure in thin soft matter films. Variation in composition, orientation, and packing motif as a function of depth are, in fact, more the rule than the exception. Examples abound, from linear and bottlebrush block copolymers, where interplays between surface energies and chain conformation lead to complex layering behaviors, to organic bulk heterojunction mixtures, where vertical segregation occurs naturally in most systems^{3,4} and is purposefully created in bilayer mixing experiments to study the miscibility of components.⁵ Vertical stratification in crystallinity and/or crystal or molecular orientation has also been reported in single component organic semiconductors.^{6,7} Ion-containing systems, such as ionic liquids, polymer electrolytes, and doped organic semiconductors also exhibit vertical stratification. In liquid crystals, orientational cues from substrates and superstrates can lead to complex orientation depth profiles. 11 In biological membranes, vertical stratification of various functional groups is not just an accidental material property, it is a key to their function. 12 Inhomogeneous film models have even been used to illuminate complex lateral processes occurring in organic photoresists.¹³ Despite the importance of vertical stratification, nondestructive tools for its evaluation are lacking.

An exciting new type of nanoscale structure control in thin films has recently been demonstrated during the physical vapor-deposition (PVD) of small molecules into oriented stable glasses. ^{14–20} High degrees of orientation and order can be achieved in this material class, even for molecular systems that do not have equilibrium crystal or liquid crystal phases. ²⁰ Anisotropic glasses have relevance to applications such as organic light-emitting diodes (OLEDs), ²¹ and the impact of glassy phases and charge transport anisotropy caused by molecular orientation within them is well-recognized in the broader organic electronics field. ²² The molecular orientation in PVD molecular glass films is largely determined by the geometry of the molecule and the substrate temperature

(T_{sub}) relative to the glass transition temperature (T_g) of the material during deposition. ^{14–20} A great deal has been learned about the control of order in these systems using bulk measures of molecular orientation, but thus far a detailed vertical depth profile has remained elusive. Orientation measurements using ultraviolet-visible (UV-Vis) or infrared (IR) spectroscopies (or ellipsometries) are sufficient to provide a bulk orientation, and we have recently shown that Near Edge X-ray Absorption Fine Structure (NEXAFS) spectroscopy can provide a surface orientation measurement, ²⁰ enabling a surface-vs-bulk comparison. However, a more complete understanding of these systems requires a vertical depth profile measurement tool with high spatial resolution and high sensitivity to molecular orientation to explore molecular-scale orientation within buried layers and at buried interfaces.

Here we provide new measurements of orientation in PVD-deposited, highly oriented posaconazole glass films using an emerging technique: polarized resonant soft X-ray reflectivity (p-RSoXR). p-RSoXR has been used to study orbital orientation and magnetic dichroism in inorganic systems; $^{23-25}$ herein we describe major advances in its application to organic films. p-RSoXR uses NEXAFS transition dipoles to derive contrast in composition and orientation. It is an extension of RSoXR (without the "p"), $^{26-29}$ where analysis of organic films has usually ignored the influence of polarization, often justified by its application to isotropic materials. In previous demonstrations on organic films, p-RSoXR was effective for measuring the bulk orientation of NEXAFS transition dipole vectors in homogenous thin films, most notably the $1s\rightarrow\pi^*$ in polymers, 30 small molecules, 31 and self-assembled monolayers. 32 In this manuscript, we develop an approach to p-RSoXR that permits complete *molecular orientation depth profiling*, allowing for the modeling and extraction of orientations simultaneously in the bulk and interfaces, and for the measurement of multilayer films having distinct orientations within sublayers. We demonstrate

how to depth profile molecular orientation using posaconazole glass films, with an emphasis on the experimental requirements and data analysis practices. We show that p-RSoXR is highly sensitive to thin, oriented surface layers, and that the orientation depth profiles for posaconazole films are consistent with expectations from the surface equilibration mechanism for imparting orientation in molecular glass films during PVD.¹⁷ Furthermore, by using a NEXAFS-informed approach to interpreting the p-RSoXR results, we extract molecular tilt values for the bulk layer of the films that quantitatively agree with IR spectroscopy results¹⁸. Finally, we demonstrate that our quantitative molecular tilt analysis can be applied to a bilayer film with orientationally distinct sublayers, revealing not only the orientation within each of the ≈ 20 nm sublayers, but also the nature of the interface between them, which is due solely to changes in orientation and cannot be resolved with existing depth profiling techniques.

Background

The world of nanostructured soft materials needs improved depth profiling techniques, as currently available depth profiling techniques have significant limitations. Destructive methods such as secondary ion mass spectrometry (SIMS)^{5,33} and sequential X-ray photoemission spectroscopy (XPS)^{9,34} rely on atomic contrast to differentiate composition, with poor contrast in organics having similar elemental ratios, such as pure hydrocarbons. These techniques also lose resolution near the film bottom due to uneven material removal. Conventional hard X-ray reflectivity (XRR) also has limited contrast in low atomic number (low-z) materials. Neutron reflectivity (NR) can leverage selective deuteration for nanometer-level resolution composition depth profiles,³⁵ but it imposes the costs and synthetic challenges of deuteration, and it requires sample uniformity over relatively large areas, which can be challenging for many applications.

SIMS, XPS, XRR, and NR are not sensitive to molecular orientation. Resonant soft X-ray reflectivity has emerged recently as a powerful depth profiling technique that is practiced similarly to XRR, except that NEXAFS resonances are used to enhance contrast for low-z materials.^{26–28} In most RSoXR studies of organic films to date, polarization has been ignored or 'worked around,' rather than exploited to extract orientation.

Variable-angle spectroscopic ellipsometry (VASE) is an accessible benchtop technique that is sensitive to molecular orientation by detecting the birefringent response of optical transition dipoles. He full orientation depth profiles obtained from VASE are limited to a depth resolution of ≈ 5 nm and are rarely published due to the challenges of developing robust optical models, but approaches for doing so are established. Using p-RSoXR to depth profile molecular orientation provides a number of advantages compared to VASE. For example, since the index of refraction at soft X-ray wavelengths only deviates slightly from unity 7, developing optical models to describe orientation-induced birefringence is greatly simplified. Additionally, the two orders of magnitude decrease in wavelength relative to VASE (UV-Vis) provides p-RSoXR with the opportunity to achieve significantly better depth resolution. Finally, the resonances (i.e., NEXAFS transition dipoles) leveraged by p-RSoXR are, in principle, resolved to a single unfilled valence orbital within a molecule, thus orientations derived from them can be separated and assigned to sub-molecular moieties. Therefore, p-RSoXR might be able to provide depth profiles that can, for instance, distinguish the backbone vs. side chain orientation in rigid rod polymers. The provide of the provide depth profiles that can, for instance, distinguish the backbone vs. side chain orientation in rigid rod polymers. The provide depth profiles that can, for instance, distinguish the backbone vs. side chain orientation in rigid rod polymers.

Experimental

Posaconazole VETRANAL analytical standard was used as received from Sigma Aldrich. Samples were prepared by PVD in a home-built vacuum chamber at a base pressure of 10⁻⁴ Pa, as

detailed in previous publications^{18,19}. Films of approximately 70 nm thickness were prepared on identical 1-inch undoped silicon <1 0 0> wafers with ≈2 nm native oxide from Virginia Semiconductor. Posaconazole film orientation was controlled by adjusting the substrate temperature during PVD, as described previously¹⁸.

NEXAFS data were collected using the Soft X-ray Spectroscopy beamline at the Australian synchrotron (AS)³⁹. Scans were performed using linearly polarized X-rays and five different sample tilt angles, such that the electric field vector was aligned at $\theta = 90^{\circ}$, 70° , 55° , 40° , and 20° relative to the sample surface normal. X-ray absorption was monitored using the channeltron detector operating in partial electron yield mode (PEY) with a bias of -218.5 V. Scans were recorded over an energy range of (230 to 430) eV. The raw data were corrected and analyzed using the Quick AS NEXAFS Tool (QANT)⁴⁰ as detailed in the supporting information.

The p-RSoXR measurements demonstrated in this work were performed at Beamline 11.0.1.2 of the Advanced Light Source (ALS) at Lawrence Berkeley National Laboratory (LBNL)^{41,42}. Preliminary p-RSoXR experiments on posaconazole films were also performed at the BEAR beamline of Elettra Sincrotrone Trieste⁴³ and the data are provided in the supporting information. At ALS beamline 11.0.1.2, reflectivity data were acquired using both s- and p-polarized X-rays. p-RSoXR measured using four different scans were X-ray energies (250.0, 283.9, 284.7, and 285.7) eV and an incident angle range of $\theta \approx 1^{\circ}$ to 60° relative to the sample plane. Spectroscopic energy scans at fixed incident-angle were also performed to qualitatively assess molecular orientation and to normalize the p-RSoXR intensity values (see supporting information). All reflectivity measurements were recorded using the CCD image detector; images were recorded using a 300x300 pixel region of interest with 2x2 binning in order to reduce readout overhead. To prevent detector saturation, the incident beam flux was attenuated by adjusting the higher-order suppressor (HOS) mirrors every $\theta \approx 5^\circ$ during the angle the scans, until the specular beam no longer saturated the detector when using the fastest shutter speed. In all cases, the two previous measurement angles prior changing the HOS setting were repeated to provide overlapping data during reduction.

The reflectivity data were reduced using Python code scripted in JupyterLab and analyzed using the ReMagX software developed by Sebastian Macke and Coworkers^{44,45}, as detailed in the supporting information. In short, the specularly reflected intensity was extracted and corrected for background counts from the CCD images recorded at each incident angle. The resulting intensity values we further corrected for changes in the instrument setup throughout the scan and normalized by the direct beam to yield absolute reflectivity data. For each sample, the non-resonant (250.0 eV) data were fitted in ReMagX to extract the total posaconazole film thickness and surface roughness, which were then fixed during subsequent analysis of the resonant data. The resonant data were fitted by adjusting the optical properties of the posaconazole film in the reflectivity model, in order to extract molecular orientation information.

Results and Discussion

Posaconazole is an ideal material system to validate novel depth profiling techniques. Previous demonstration has revealed that the molecular orientation in posaconazole films can be controlled by tuning the substrate temperature (T_{sub}) during PVD.¹⁸ Posaconazole molecules are thought to behave in a rod-like fashion, where the average long-axis tilt within a film can adopt a net horizontal, net vertical, or isotropic orientation. PVD conditions leading to these bulk orientations were identified using infrared (IR) and VASE analysis: $T_{sub} \ll T_g$ yields horizontal orientation, $T_{sub} \ll T_g$ provides vertical orientation, and $T_{sub} \ge T_g$ results in an isotropic film, similar to a liquid-

cooled glass.¹⁸ To demonstrate how p-RSoXR can be used to extract molecular orientation depth profiles, we characterize three posaconazole films (T_g = 330 K)¹⁸ that were prepared with distinct bulk orientations: (i) horizontal (T_{sub} = 290 K), (ii) vertical (T_{sub} = 327 K), and (iii) isotropic (T_{sub} = 334 K). The VASE-derived bulk film orientation for each of the samples was confirmed to be consistent with the results from Gómez et al¹⁸ (supporting information, Figure S2). We begin our study by examining the NEXAFS spectroscopy of posaconazole, as it forms the basis for orientational contrast in the p-RSoXR technique. We then provide the experimental p-RSoXR results obtained for each of the three films and show how NEXAFS-informed interpretation of p-RSoXR data can yield quantitative molecular tilt values. Finally, we demonstrate the true potential of molecular orientation depth profiling by using p-RSoXR to characterize a posaconazole bilayer stack, where the sublayers of the film are compositionally identical but orientationally distinct.

Impact of Molecular Orientation on Soft X-ray Optical Properties

A quantitative description of p-RSoXR requires understanding the resonant, anisotropic index of refraction of the material, which we develop based on NEXAFS spectroscopy. NEXAFS spectroscopy is typically applied using soft X-rays to measure the orientation and composition of organic layers, ⁴⁶ most commonly at the carbon K-edge. NEXAFS is most commonly measured in electron yield (EY) modes, which provide the composition and orientation near the film surface. Fluorescence and transmission NEXAFS can deliver a bulk composition and/or orientation measurement, but they are more rarely employed because they are more experimentally challenging. The closest approach to a molecular orientation depth profile that can be accomplished using the various modes of NEXAFS alone is a surface vs. bulk comparison;

however, we demonstrate how quality NEXAFS data plays a key role in enabling p-RSoXR to provide quantitative molecular tilt values.

Carbon K-edge NEXAFS resonances are due to the excitation of 1s electron from a carbon center into an unfilled (typically π^* or σ^*) molecular orbital that includes the carbon center of the initial state. Peaks in NEXAFS spectra can typically be assigned to carbon centers within specific moieties or bonds of a molecule. In Figure 1a we show the chemical structure of posaconazole, and in Figure 1b,c we show a partial electron yield (PEY) carbon K-edge NEXAFS spectrum (gray circles) from the vertical posaconazole sample, along with a multi-peak fit (black curve). We recently assigned a number of resonant peaks due to 1s $\rightarrow \pi^*$ transitions in posaconazole to specific carbon centers (shown below the data in Figure 1b,c);²⁰ the carbon centers associated with these assignments are highlighted on the molecular structure in Figure 1a. In all cases, the dipole moments of these 1s $\to \pi^*$ transitions are expected to be perpendicular to the planes of their respective ring moiety⁴⁶. The measured resonant peak intensity will vary proportionally to the dot product of the incident electric field vector and the resonating transition dipole. As demonstrated in Figure 1d,e, when the electric field vector is varied by adjusting the incident angle of the X-ray beam between 20° and 90°, the NEXAFS spectra collected from the vertical posaconazole sample (T_{sub} = 327 K) shows monotonic changes in peak intensity, indicative of orientation anisotropy at the film surface.

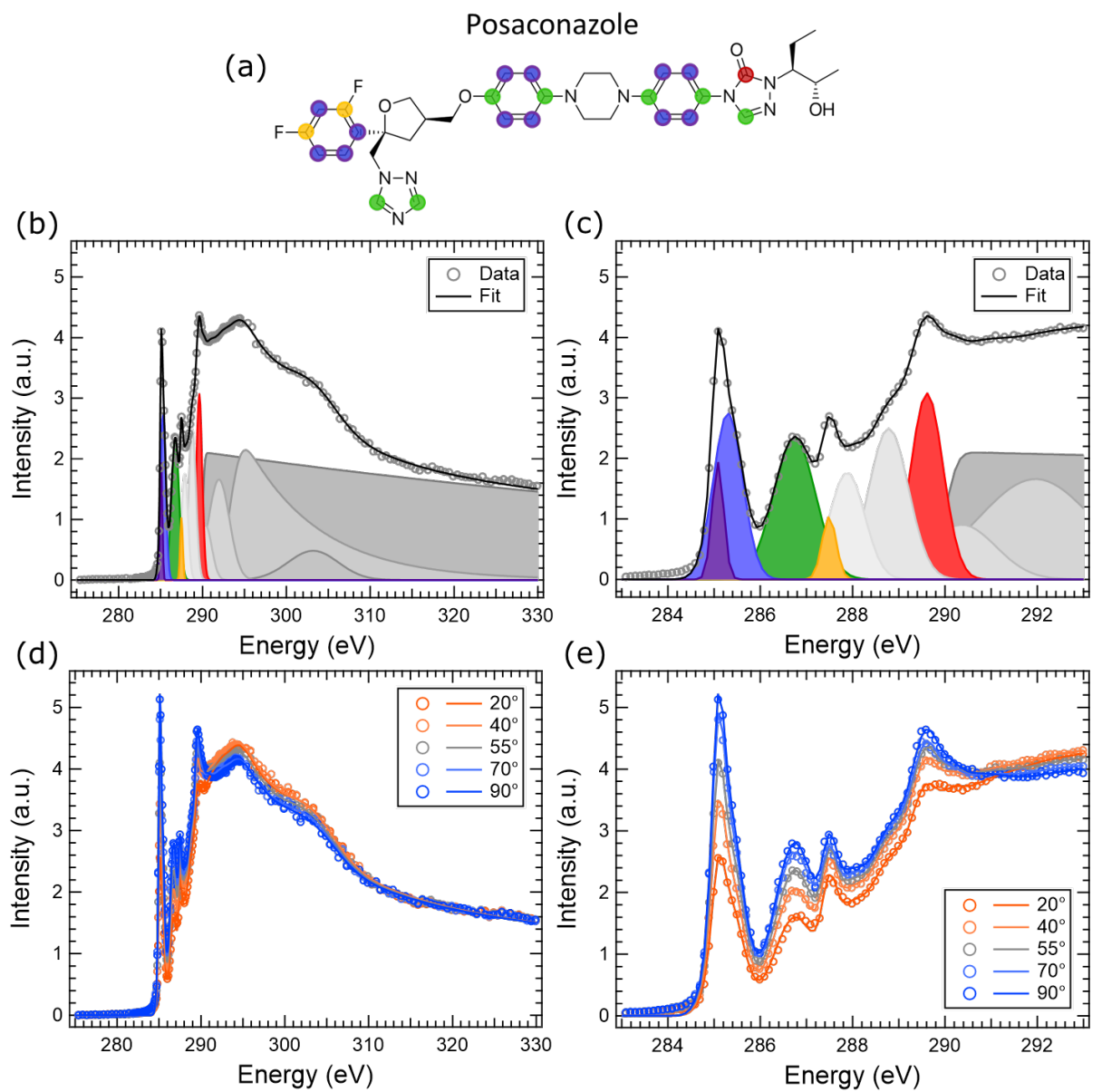


Figure 1: (a) Chemical structure of posaconazole with carbon atoms that exhibit $1s \rightarrow \pi^*$ NEXAFS transitions highlighted. The highlight colors correspond to the unique peak features fit to the (b,c) orientation-insensitive magic angle PEY-NEXAFS spectrum (54.7° angle between electric field vector and sample normal) from the vertical ($T_{\text{sub}} = 327 \text{ K}$) sample. In (b,c), the open gray circles represent the data and the solid black curve represents the multi-peak fit to the data. The individual peaks and step edge feature used to generate the fit are shown offset below the data. The purple (285.1 eV) and blue (285.3 eV) peaks correspond to $1s \rightarrow \pi^*(C=C)$ resonances from the phenyl rings; the green (286.7 eV) peak corresponds to the $1s \rightarrow \pi^*(C=C)$ and $1s \rightarrow \pi^*(C=N)$ resonances from the phenyl and triazole(one) rings; the gold (287.5 eV) peak corresponds to the $1s \rightarrow \pi^*(C=C)$ resonance from the fluorinated phenyl ring; and the red (289.6 eV) peak corresponds to the $1s \rightarrow \pi^*(C=C)$ resonance of the triazolone ring. (d,e) Post-edge normalized PEY-NEXAFS spectra from the vertical sample measured with varying incident angles between 20° and 90°. The open circles represent the data and the solid curves represent the multi-peak fits to the data.

Qualitative inspection of the $1s \rightarrow \pi^*$ region ($\approx 284 \text{ eV}$ to $\approx 289 \text{ eV}$) of the NEXAFS spectra from the vertical sample (Figure 1e) suggests each resonance has similar orientation, i.e., the highest intensity for each peak is observed at 90° incidence, and the lowest intensity is at 20° incidence. However, after using multi-peak fitting to deconvolute the spectra, we find different extents of dichroism across the $1s \rightarrow \pi^*$ region. The peak at 285.1 eV (phenyl) exhibits the strongest dichroism, followed by the peaks at 285.3 eV and 286.7 eV (phenyl/triazole), which have roughly similar dichroism. The intensity of the 287.5 eV (fluorinated phenyl) peak does not change with incident angle, implying isotropic orientation. The unassigned 287.9 eV, 288.8 eV, and 290.4 eV peaks exhibit similar dichroism to the 289.6 eV (carbonyl) peak, with each showing less dichroism than the phenyl/triazole peaks.

To relate the measured dichroism of the $1s \rightarrow \pi^*$ transition dipoles to the extent of 'vertical' orientation of a posaconazole molecular long axis, we must make some assumptions about the conformations and symmetries adopted by the posaconazole molecule. We first assume that the posaconazole molecules, or at least a central 'core' of several ring systems, are rod-like⁴⁷, as depicted in Figure 2a,b. We then assume that since there are no crystalline phases present to constrain molecular packing, any rotation about the long axis is equally probable within the glass, as shown in Figure 2c. This assumption allows us to describe the core $1s \rightarrow \pi^*$ transition dipole as a planar rather than vector orbital, adopting the nomenclature described by Stöhr (specifically referring to Fig 9.3 and Eq 9.17 in Ref ⁴⁶). The extent of $1s \rightarrow \pi^*$ transition dipole dichroism thus describes the rod-like long axis orientation explicitly. We also employ the common assumption that a net in-plane isotropic distribution of micro- or nanoscale domains exist within the measured sample volume, thus providing arbitrary rotations about surface normal, as shown in Figure 2d. Finally, we assume (not depicted) that the various $1s \rightarrow \pi^*$ systems in the oriented molecular core

will have slightly different degrees of tilt relative to the long axis, but that some systems will be more perfectly perpendicular to the long axis orientation than others. Under these assumptions, less perfectly perpendicular resonant systems would exhibit less peak dichroism in oriented samples. We choose the peak at 285.1 eV (phenyl), which exhibits the strongest dichroism, to describe long axis orientation.

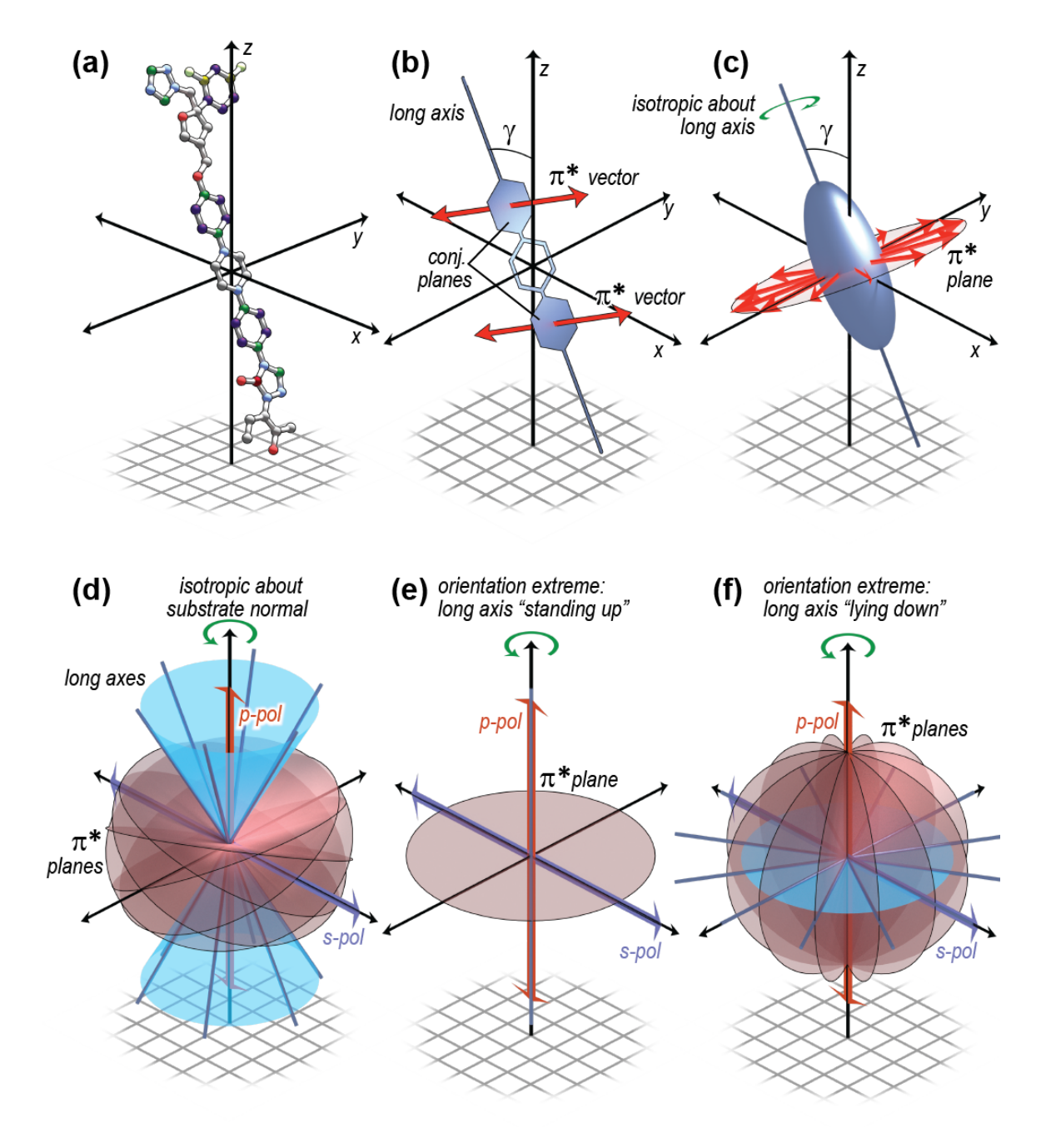


Figure 2: Figure showing symmetry of posaconazole transition dipoles and defining geometry of p-RSoXR and NEXAFS setup/coordinate system.

To quantify the average long axis tilt from the 285.1 eV (phenyl) peak dichroism, we use Equation 1, which is adapted from Stöhr's ⁴⁶ Eq 9.17a:

$$A_{peak} = C * \left\{ 1 - \frac{1}{4} [3\cos^2(\theta) - 1][3\cos^2(\gamma) - 1] \right\}$$
 (1)

where A_{peak} is the peak area, θ is the X-ray incident angle, γ is the planar tilt (see Figure 2b,c), and C is a constant corresponding to the peak area for an isotropic sample. Using the peak areas extracted from the NEXAFS data shown in Figure 1d,e, we find that the average posaconazole molecular tilt, $\langle cos^2\gamma \rangle$, at the surface of the vertical sample corresponds to $\gamma = 32.9^{\circ} \pm 1.4^{\circ}$, assuming a narrow distribution of γ , consistent with a nominally vertical orientation. Throughout the manuscript we will adopt the assumption of a narrow distribution and report $\langle cos^2\gamma \rangle$ as simply γ . We note that an isotropic sample will thus have $\gamma = 54.7^{\circ}$. Similar NEXAFS analysis was performed on the horizontal and isotropic samples, and the results for all three films are provided in Figure S3 of the supporting information.

Our assumption of high symmetry about surface normal (see Figure 2) means that the optical properties of oriented posaconazole can be treated as uniaxial, with distinct in-plane (x,y) and out-of-plane (z) contributions to the index of refraction. We use the common expression of index of refraction for X-ray wavelengths ($n = 1 - \delta + i\beta$), where 1- δ is the real component of the index of refraction and β is the imaginary component, which gives rise to absorption. For uniaxial systems, the in-plane contributions are represented by δ_{xx} and β_{xx} (xx and yy are equivalent), whereas the out-of-plane contributions are given by δ_{zz} and β_{zz} . In Figure 3 we provide the uniaxial components of the complex index of refraction for posaconazole with an average tilt of $\gamma = 32.9^{\circ}$, based on the NEXAFS data from the surface of the vertical sample shown in Figure 1 (see Methods

for details). Figure 3a shows that the vertical sample surface exhibits significant β -dichroism (β_{xx} - β_{zz}), which is calculated and plotted in Figure 3b. The origin of β -dichroism for a vertical sample is illustrated in Figure 2e, where it is shown that the π^* orbital plane aligns with the sample plane (x-y). Thus, when the electric field vector of incident radiation is aligned with the x-y plane (i.e., s-polarization, s-pol), absorption (β_{xx}) due to π^* resonances is maximized. Likewise, when the electric field vector of incident radiation is aligned with the z-axis (i.e., p-polarization, p-pol), absorption (β_{zz}) due to π^* resonances is minimized, and the resulting β -dichroism is positive for the π^* resonances. Similar geometric arguments can be used to predict the β -dichroism for posaconazole films with horizontal orientation (Figure 2f). In this case, the π^* orbital plane is aligned with the z-axis, thus out-of-plane absorption (β_{zz}) is maximized, whereas in-plane absorption (β_{xx}) is minimized because only half of the possible configurations from the azimuthal average align with the s-pol electric field vector. Thus, horizontally oriented posaconazole films will exhibit negative β -dichroism for the π^* resonances.

The orbital alignment that leads to the β -dichroism seen in Figure 3b also induces birefringence in the real component of the index of refraction, δ . We calculate δ_{xx} and δ_{zz} (Figure 3c) using the Kramers-Kronig (KK) relations with the β -spectra shown in Figure 3a. Birefringence is clearly seen in Figure 3c and quantified in Figure 3d (in this work, we define δ -birefringence as the negative of $[\delta_{xx} - \delta_{zz}]$, in order to provide consistency in sign with the β -dichroism for the strongest resonance near 285 eV). Unlike β -dichroism, the energy-dependence of δ -birefringence cannot be explained though simple geometric arguments. For instance, the sign of δ -birefringence for the vertical sample changes multiple times within the $1s \rightarrow \pi^*$ resonance energy region (≈ 284 eV to ≈ 289 eV) and the maximum δ -birefringence value occurs ≈ 0.3 eV below the peak absorption

resonance at 285.1 eV; however, there is still a direct correlation between δ -birefringence and average molecular tilt, such that it can be used to extract molecular orientation.

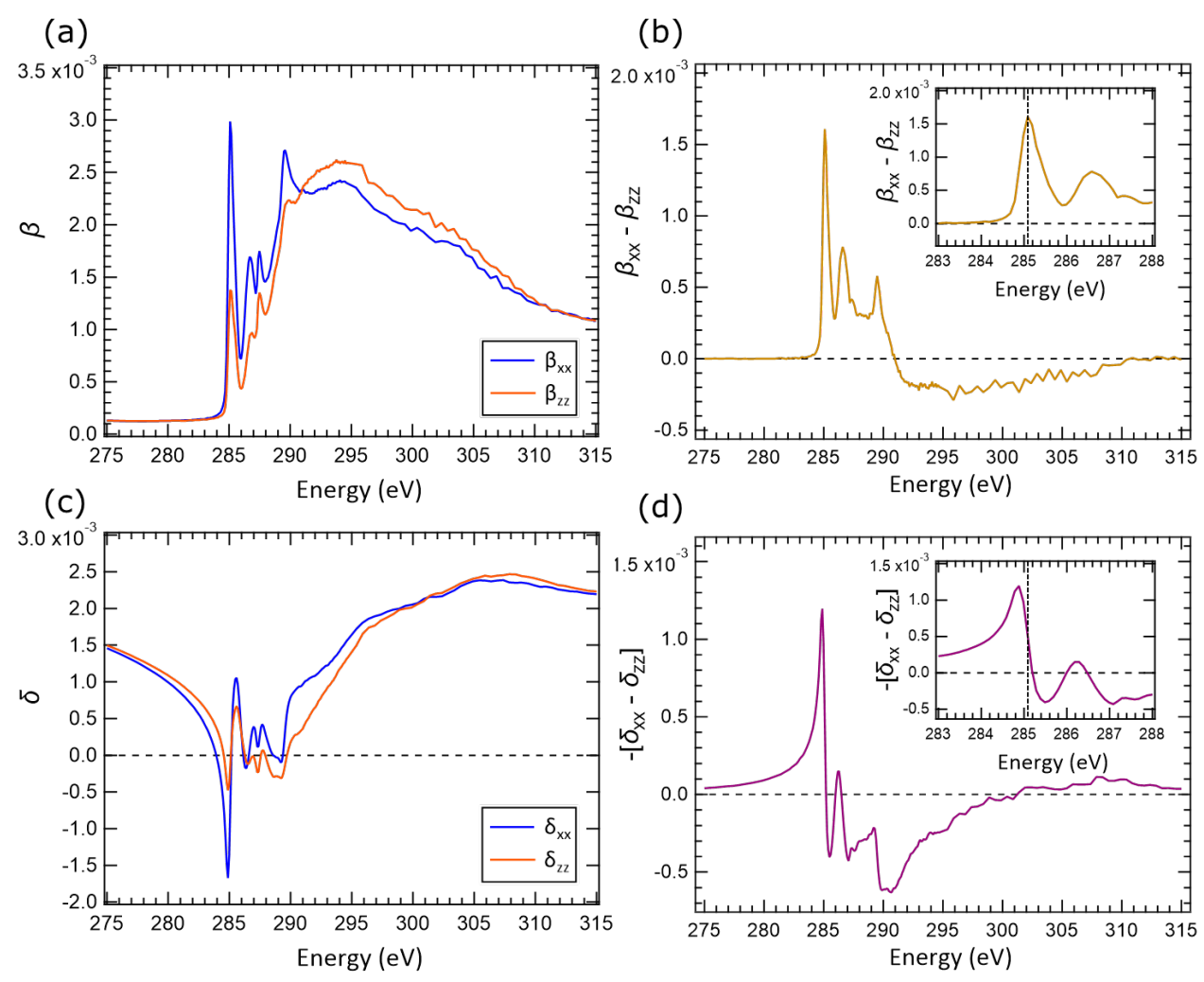


Figure 3: (a) Imaginary components (β) of the complex index of refraction for posaconazole from the surface of the vertically aligned ($T_{sub} = 327 \text{ K}$) sample. (b) The corresponding β -dichroism. (c) The KK-calculated real components (δ) of the complex index of refraction based on of the imaginary components in (a). (d) The corresponding δ -birefringence.

Unlike NEXAFS, which nominally only probes absorption (β), p-RSoXR is sensitive to both δ (primarily through interference between the various reflected waves) and β (through absorption)³⁷. Detecting changes in δ (and thus potentially δ -birefringence) provides the opportunity to decouple orientation sensitivity from absorption, which is essential for orientation depth profiling. For

example, if we rely solely on β -dichroism to probe posaconazole tilt, then to maximize our orientation sensitivity we would make p- RSoXR measurements at 285.1 eV; however, due to the strong absorption at that energy, a 70 nm thick posaconazole film would transmit less than 10 % of the reflected beam for incident angles less than 25°, drastically minimizing the information content of the p-RSoXR data. If, on the other hand, we use δ -birefringence to extract posaconazole tilt, then we can make our p-RSoXR measurement using 284.7 eV X-rays, which still have a strong sensitivity to orientation, but due to lower absorption, transmit at least 10 % of the reflected beam for all incident angles greater than 3.6°. With these insights in mind, we select energies for p-RSoXR measurements that provide significant δ -birefringence, while also avoiding strong absorption. Furthermore, to increase confidence in assigning molecular orientation from δ -birefringence, we performed measurements at energies where vertical orientation yields positive δ -birefringence (283.9 eV and 284.7 eV) as well as negative δ -birefringence (285.7 eV) based on the NEXAFS-derived spectrum in Figure 3d.

p-RSoXR Analysis of single-layer films

Representative p-RSoXR data from the isotropic (T_{sub} = 334 K) single-layer posaconazole film are shown in Figure 4. In Figure 4a we provide the reflectivity data collected using both s- and p-polarized (s-pol, p-pol) 250 eV X-rays, which are far lower in energy than the carbon K-edge and thus do not exhibit resonant effects, i.e., the index of refraction anisotropy is negligible. We use the data (open circles) in Figure 4a to extract the film geometry, specifically the posaconazole film thickness and the interfacial width at the free surface, which describes sample roughness. The model used to fit the data assumes the bare-atom index of refraction for posaconazole (see supporting information for details). As shown in Figure 4a, the simultaneous fit (solid curves) to

the data recorded using both X-ray polarizations is in excellent agreement with the data. The principal difference between this result and a hard X-Ray reflectivity measurement, which would also be non-resonant, is the p-polarized feature near $q = 0.18 \text{ Å}^{-1}$, which is due to Brewster's angle where reflectance vanishes. For soft X-rays interacting with isotropic media, Brewster's angle occurs near $\theta \approx 45^{\circ}$. The Brewster's angle feature has limited previous analysis of organic films using p-RSoXR³⁰ because the intensity of the p-pol reflectivity can become orders of magnitude lower than that of the s-pol reflectivity, requiring a detector with much higher dynamic range, or a high flux X-ray source that can be accurately attenuated. As shown in Figure 4a, we are able to overcome this challenge and achieve ≈ 7 orders of dynamic range at ALS beamline 11.0.1.2 by using the CCD detector and attenuating the incident flux with the higher order suppressor (HOS) mirrors, providing suitable data near and beyond the Brewster's angle minimum in the 250 eV data. For reference, we highlight the experimental "noise floor" in each of the p-RSoXR plots, which represents approximately the lowest experimental reflectivity that can be distinguished from the background intensity for the configuration and X-ray energy being used. Our analysis of resonant p-RSoXR data, below, will demonstrate the importance of p-pol data near Brewster's angle when attempting to extract molecular orientation depth profiles.

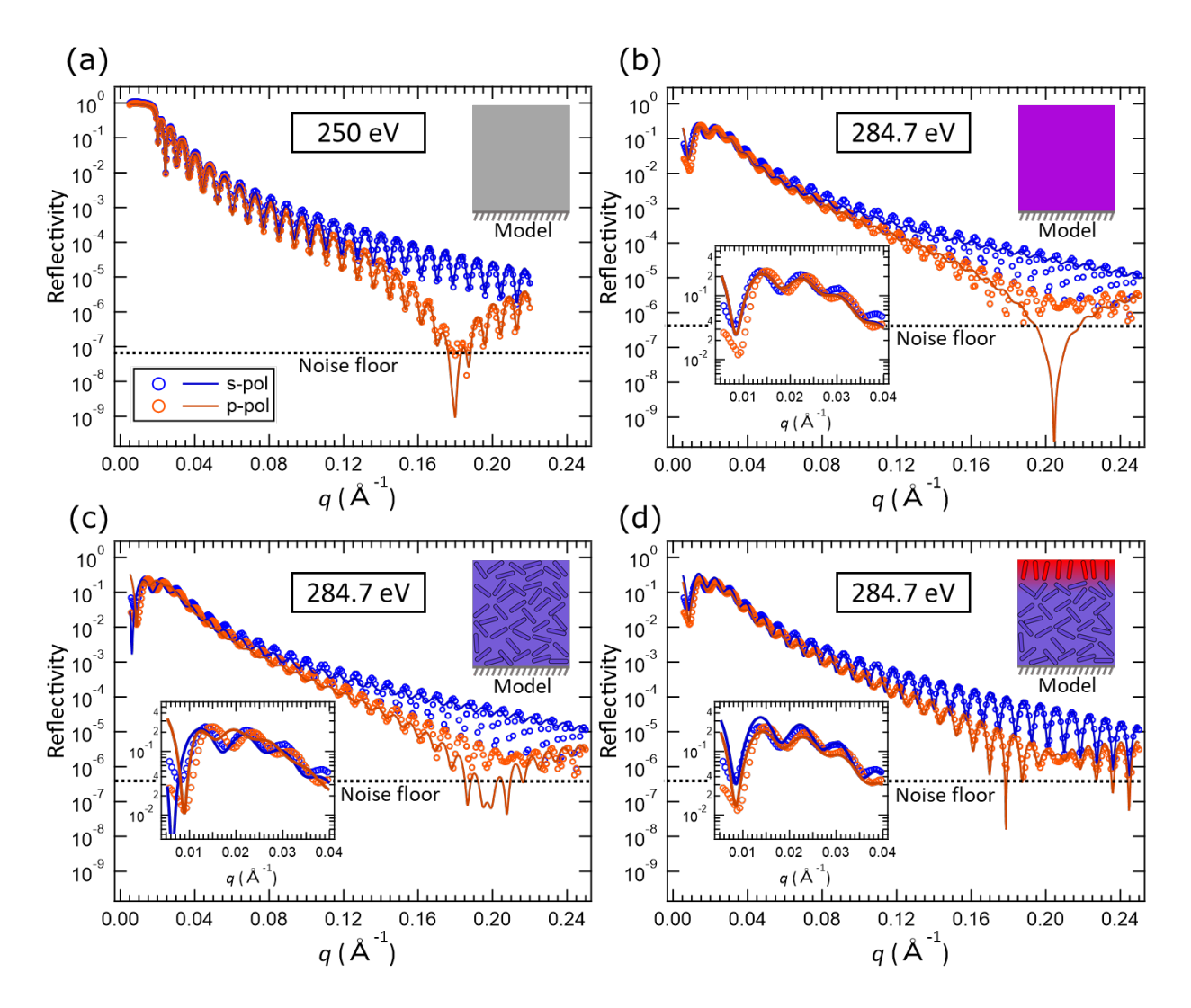


Figure 4: p-RSoXR data collected from the isotropic posaconazole sample deposited at Tsub = 334 K. In each plot, blue circles and curves correspond to s-pol data and fits, respectively, and the orange circles and curves correspond to the p-pol data and fits. In all cases, the s- and p-polarized data are fit simultaneously using a single optical tensor for each layer in the model. (a) non-resonant (250 eV) data fit by adjusting film geometry and using the bare-atom index of refraction for a $\rho = 1.22$ g/cm3 posaconazole film. (b) resonant (284.7eV) data fit by adjusting the complex index of refraction for an isotropic optical tensor. (c) resonant (284.7eV) data fit by adjusting the uniaxial dielectric tensor. (d) resonant (284.7eV) data fit by modeling the posaconazole film with two distinct layers and adjusting the layer thickness ratio, uniaxial dielectric tensors, and interfacial widths. In fits shown in (b-d), the total film thickness and the surface roughness were fixed based on the values extracted from the model fit in (a).

In Figure 4a, the only difference between the s-pol and p-pol data is the magnitude of the reflectivity as Brewster's angle is approached; the critical angle and the location of the fringe

oscillations are unaffected by polarization because there is negligible δ -birefringence or β dichroism at 250 eV (regardless of posaconazole orientation). The presence of δ -birefringence will cause a shift in the location of the critical angle and subsequent fringe oscillations, as well as potentially affecting the fringe amplitude when comparing s-pol and p-pol data, while β -dichroism will cause differing levels of attenuation between the s-pol and p-pol data, typically manifesting as changes in reflected intensity at low angle (low q) and differences in fringe oscillation amplitude. In Figure 4b-d, we show p-RSoXR data (open circles) collected from the isotropic posaconazole film at 284.7 eV, a resonant condition that shows strong sensitivity to orientation in δ -birefringence. It is immediately apparent that resonant effects change the reflectivity data dramatically when compared to the 250 eV data; there is no region of total external reflection at low q-values (and thus no critical angle), and the p-pol data does not exhibit a Brewster's angle minimum that approaches zero at $\theta \approx 45^{\circ}$ ($q \approx 0.205 \text{ Å}^{-1}$). Furthermore, close inspection of the lowq data in the inset of Figure 4b reveals that there is a slight offset in fringe location, as well as a difference in reflected intensity between the two polarizations, suggesting there is orientation anisotropy within the film. In Figure 4b-d, we demonstrate how changing the optical model of the posaconazole film during p-RSoXR fitting analysis impacts the goodness of fit, and thus our ability to extract molecular orientation from the data.

In Figure 4b we show the best-fit depth profiles (solid curves) when using a simple single layer model with an isotropic dielectric tensor to represent the posaconazole film. To reduce the number of free parameters during fitting, we fixed the geometry (film thickness and surface roughness) to the results from the 250 eV fit and allowed only the isotropic dielectric tensor parameters (δ and β) to vary. It is clear from the fit curves in Figure 4b that any isotropic tensor, which will produce a Brewster's angle minimum in the p-pol data near $q \approx 0.2 \text{ Å}^{-1}$, cannot be used to model the resonant

reflectivity data. Therefore, we must introduce posaconazole orientation into the model, even though the posaconazole film is isotropic in VASE (see supporting information, Figure S2).

The solid curves in Figure 4c represent the best-fit profiles when the posaconazole film is modeled as a single layer with optical properties described by a uniaxial dielectric tensor. The geometry parameters are still fixed to the fit from the 250 eV data, while the components of the uniaxial dielectric tensor were allowed to vary. The fit shows an improvement in capturing some of the qualitative features of the p-RSoXR data compared to the isotropic model in Figure 4b. Most notably, the Brewster's angle minimum is suppressed. It is not an excellent fit, however. The location of fringe oscillations in the p-pol data at low *q*-values (Figure 4c, inset), as well as the fringe amplitude in both polarizations are significantly different than the data. The results from Figure 4b-c clearly indicate that a single-layer model cannot be used to describe the optical properties of the posaconazole film at resonant energies. We must include additional layers. It is known that posaconazole films can have a different free surface orientation than the bulk.²⁰ A second layer on top of the bulk film would be consistent with those results.

Our third model highlights the sensitivity of p-RSoXR to thin, oriented surface layers. The fit curves shown in Figure 4d model the posaconazole film as two layers, both of which have independent uniaxial dielectric tensors. This two-layer model quantitatively captures the experimental data from both polarizations over the entire q-range measured. Moreover, the model parameters for the fit shown in Figure 4d indicate that there is a vertically oriented surface layer on top of a nearly isotropic bulk film, which is consistent with the observations from both VASE (bulk) and NEXAFS (surface) (Supporting Information Figures S2, S3). However, unlike the combined VASE+NEXAFS analysis, the p-RSoXR analysis provides the thickness and interfacial width of the vertically-oriented surface layer; the best-fit thickness of the surface layer is 1.5 nm

and the transition between bulk and surface orientation occurs abruptly (i.e., the best-fit interface width is 0 nm). The thickness of the surface layer is on the order of posaconazole's molecular dimensions, indicating the presence of an oriented monolayer at the free surface of the isotropic posaconazole film. To our knowledge, this represents the first experimental measurement to yield the depth dependence of orientation at the free surface of an organic glass. Interestingly, the molecular-scale dimensions of the surface layer and the abrupt transition to the bulk film orientation is consistent with the simulated equilibrium surface structure of other rod-like molecular glasses.¹⁹

The same analysis demonstrated in Figure 4 was performed on p-RSoXR data collected from the isotropic film using 283.9 eV and 285.7 eV X-rays. Furthermore, we collected and analyzed p-RSoXR data from the horizontal and vertical single-layer films using the same set of energies (see the supporting information for all data and analysis). In all cases, the best fit to the resonant data was obtained when using a two-layer model for posaconazole (e.g. Figure 4d). We note that extending our analysis to include a differently-oriented posaconazole bottom layer at the substrate surface did not result in significant improvements to the fits of the p-RSoXR data, suggesting the bulk orientation is unperturbed by the substrate; however, confirming such a conclusion will require additional studies to assess the p-RSoXR sensitivity limits toward buried layers of molecular dimensions.

In Figure 5, we provide the resonant (284.7 eV) p-RSoXR data (open circles) and best fit profiles (solid curves) for the isotropic, horizontal, and vertical single-layer films (Figure 5a-c), along with their corresponding δ -birefringence depth profiles (Figure 5d-f). Although all three films have similar thicknesses and are composed of the same material, their p-RSoXR data demonstrate marked differences. For example, when comparing the location of fringe maxima in the low-q

portion of the data, the horizontal (Figure 5b inset) and vertical (Figure 5c inset) samples show clear offsets between s-pol and p-pol data, whereas the fringe locations in the s-pol and p-pol data from the isotropic sample (Figure 5a inset) are almost overlapping. These shifts in fringe location with polarization are due to orientation-induced δ -birefringence, consistent with net orientation in the horizontal and vertical films. In addition to the differences observed in the low-q data between each sample, there is a notable discrepancy in the high-q data of the vertical sample (Figure 5c); rather than exhibiting a Brewster's angle minimum near $q \approx 0.2 \text{ Å}^{-1}$, the p-pol data exhibits a weak local maximum and the s-pol data has a local minimum (similar anomalous high-q behavior is also seen in the 283.9 eV and 285.7 eV data from the vertical sample, supporting information Figures S16, S18). Previous characterization of vertical posaconazole films has revealed the presence of smectic-like ordering that causes a diffraction peak at $q_z \approx 0.2 \text{ Å}^{-1}$ in grazing incidence X-ray diffraction (GIXD) measurements.²⁰ We attribute the unusual high-q behavior in the vertical sample p-RSoXR data to diffraction effects. This attribution is supported by qualitative agreement between the data and a simple multi-layer model in the supporting information (Figure S19). Because quantitative modeling of these diffraction effects is beyond the scope of this work, we exclude the data in the shaded region of Figure 5c during fitting. Excluding high-q data reduces our sensitivity to the structural details of thin oriented layers, such as the surface layers in the isotropic sample (Figure 4d), but it should not significantly impact the results for the bulk layer.

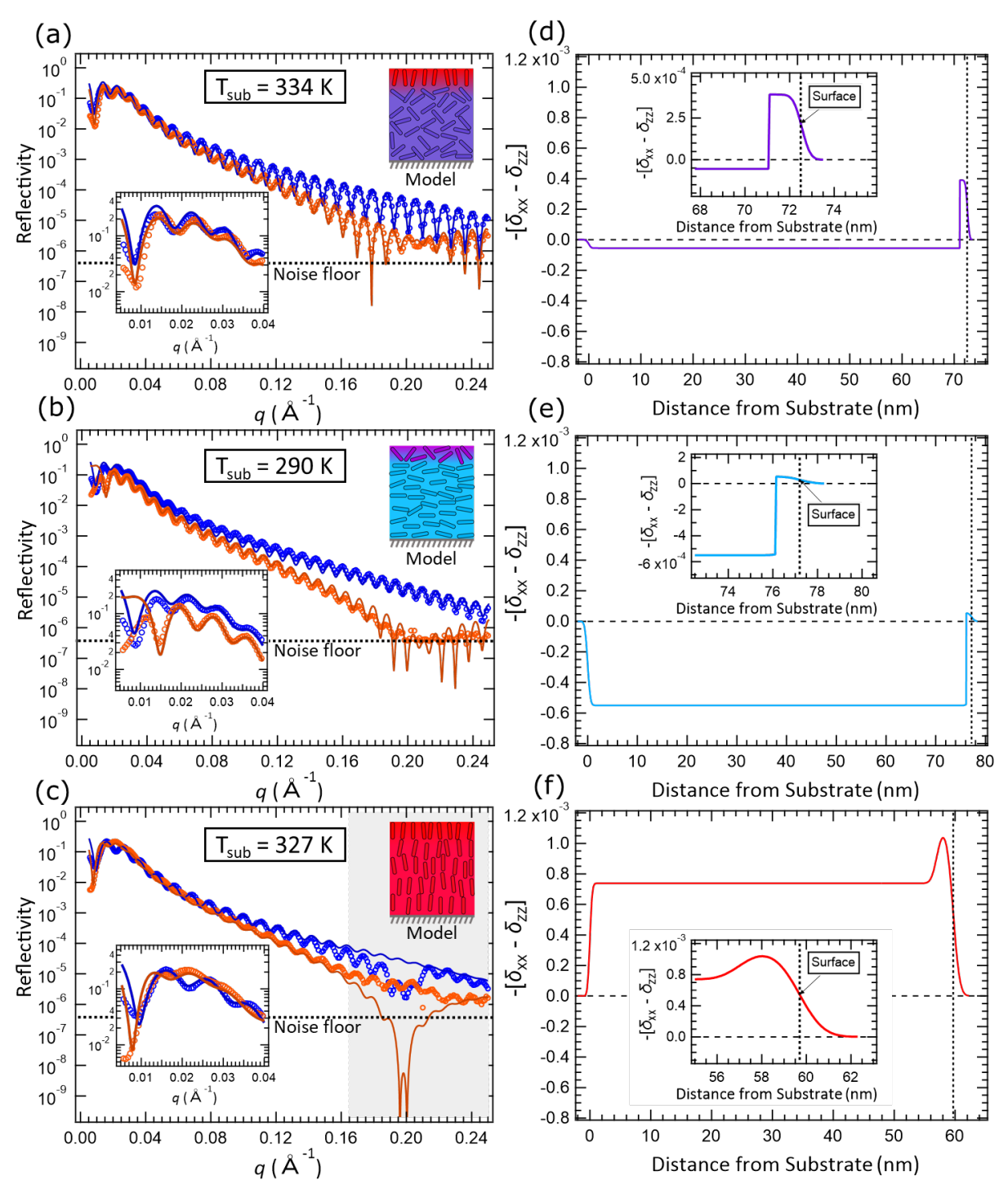


Figure 5: (a-c) p-RSoXR data collected from the (a) isotropic, (b) horizontal, and (c) vertical posaconazole single-layer films using 284.7 eV X-rays. In each plot, blue circles and curves correspond to s-pol data and fits, respectively, and the orange circles and curves correspond to the p-pol data and fits. The insets in (a-c) highlight the low-q portion of the p-RSoXR data. (d-f) depth profiles of the δ-birefringence values extracted from the fitted p-RSoXR data in (a-c), where (d) corresponds to the isotropic sample, (e) is from the horizontal sample, and (f) corresponds to the vertical sample. The insets in (d-f) highlight the free surface.

The model parameters extracted from the fits demonstrated in Figure 5a-c allow us to quantify the depth-dependence of δ -birefringence, as shown in Figure 5d-f. At a fixed energy, the sign of δ -birefringence indicates the direction of molecular orientation. For example, at 284.7 eV, a positive δ -birefringence indicates vertical orientation (see Figure 3d), whereas negative δ birefringence indicates horizontal orientation. The magnitude of δ -birefringence also trends monotonically with the extent of orientation. Therefore, the δ -birefringence depth profiles provided in Figure 5d-f can be qualitatively interpreted as orientation profiles, where a value of zero indicates random (isotropic) orientation, a positive value denotes vertical orientation, a negative value indicates horizontal orientation, and the magnitude of each value indicates the degree of tilt, i.e., larger positive values approach $\gamma = 0^{\circ}$ (perfectly vertical), and larger negative values approach $\gamma = 90^{\circ}$ (perfectly horizontal). It is notable that the δ -birefringence values for the bulk layers in each of the depth profiles in Figure 5d-f indicate molecular orientations that are consistent with the film orientations determined by VASE analysis (see supporting information, Figure S2). The δ -birefringence depth profiles for all three samples also indicate the presence of a thin surface layer more vertical than the bulk. In the cases of the isotropic (Figure 5d) and vertical (Figure 5f) samples, the surface layer orientation is vertical; however, the orientation of the surface layer on the horizontal sample (Figure 5e) is nearly isotropic. This result suggests that the molecules at the free surface of the horizontal film are frustrated between the horizontal bulk orientation and the equilibrium vertical orientation²⁰ prior to vitrification. The isotropic surface layer indicated by the δ -birefringence depth profile in Figure 5e explains the unexpected nearly isotropic posaconazole orientation measured by NEXAFS analysis of the horizontal sample (Supporting Information, Figure S3).

Quantification of molecular tilt

Although δ -birefringence provides a quantitative measurement of orientation, its conversion into molecular tilt is not immediately obvious and it will vary depending on the material. Our approach to quantifying tilt involves leveraging results from NEXAFS. We first check the consistency between p-RSoXR and NEXAFS by comparing in Figure 6 the two components of the index of refraction (β , δ) measured by p-RSoXR with the same components derived from NEXAFS, all for the vertical sample bulk. The NEXAFS-derived spectra in Figure 6 correspond to posaconazole with an average tilt of $\gamma = 32.9^{\circ}$, as γ is defined in Figure 2c. We expect the surface-sensitive NEXAFS to be similar to the bulk layer from p-RSoXR due to the characteristics of the depth profile in Figure 5f. In Figure 6a-b, we confirm that the β values from p-RSoXR are consistent with those from NEXAFS. In Figure 6c, however, we observe a systematic offset between δ values from p-RSoXR-and those from NEXAFS. This offset likely stems from error in the NEXAFS data used to perform the KK-calculations. In particular, the NEXAFS post-edge intensity is subject to systematic errors from both data acquisition (charging effects) and the assumptions used during normalization. Because these errors are systematic, their effects are mitigated by taking the difference of δ -values (i.e., calculating δ -birefringence), and in Figure 6d, we again confirm good agreement between the δ -birefringence from p-RSoXR-fitted and that from NEXAFS.

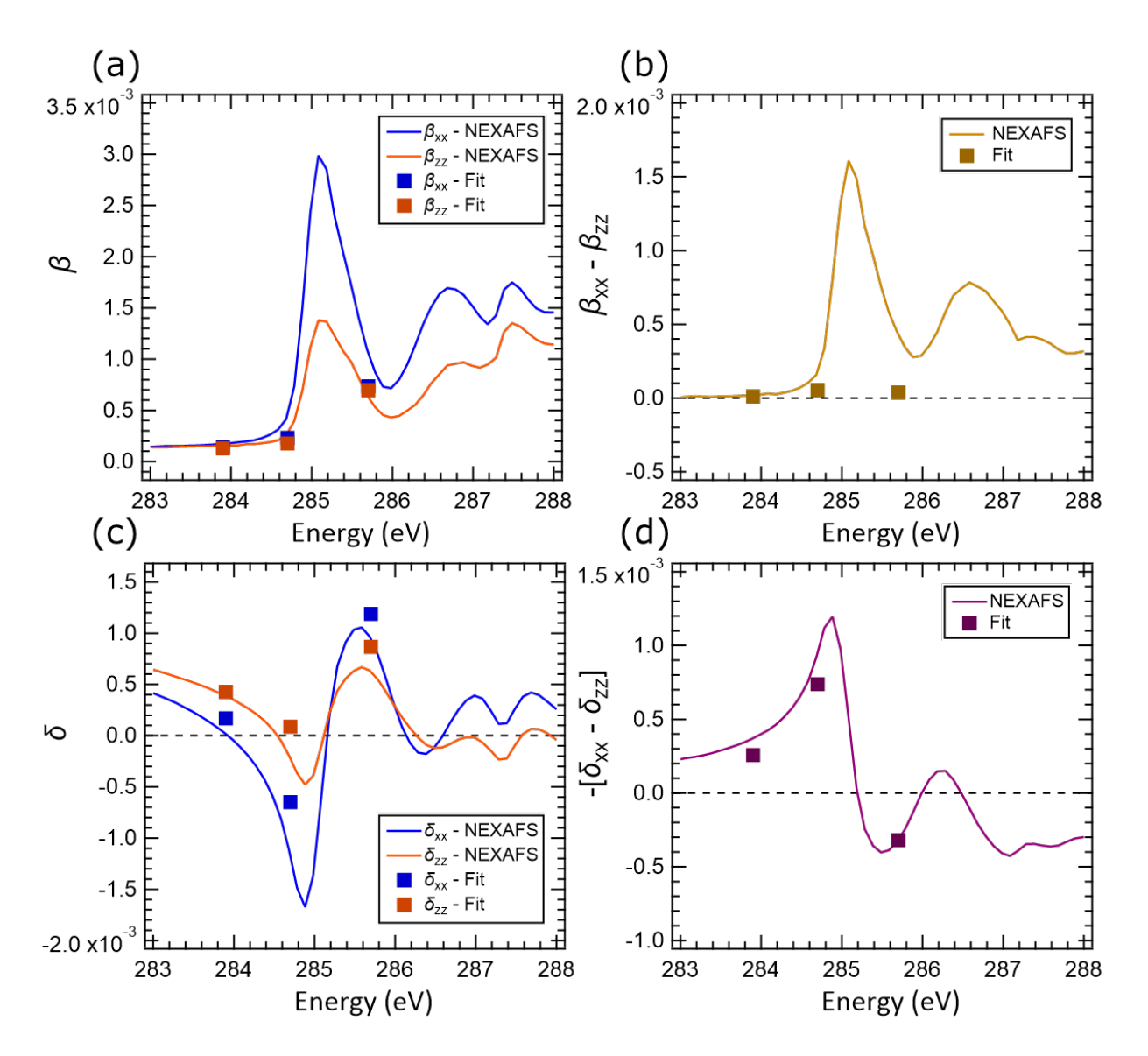


Figure 6: (a) Comparison of the β-values determined from the variable incident-angle PEY-NEXAFS and the fitted p-RSoXR data for the Tsub = 327 K sample. Blue curves and symbols correspond to the in-plane absorption (β_{xx}), and the orange curves and symbols correspond to the out-of-plane (β_{zz}) values. (b) the corresponding β-birefringence calculated from the data in (a). (c) Comparison of the δ-values determined from the variable incident-angle PEY-NEXAFS data through the KK-relations and the fitted p-RSoXR data for the T_{sub} = 327 K sample. Blue curves and symbols correspond to the in-plane absorption (δ_{xx}), and the orange curves and symbols correspond to the out-of-plane (δ_{zz}) values. (d) the corresponding δ-birefringence calculated from the data in (c).

The quantitative consistency between p-RSoXR-fitted and NEXAFS-calculated δ -birefringence values in Figure 6d suggests that a framework can be developed for converting the δ -birefringence to meaningful and quantifiable molecular tilt values (γ). We illustrate such a framework in Figure 7. In Figure 7a, the solid symbols correspond to the p-RSoXR-fitted δ -birefringence values extracted from the bulk layer of each posaconazole film analyzed in Figure 5, and each curve corresponds to the expected δ -birefringence for posaconazole with a specific γ -value, as calculated from the experimental NEXAFS spectra (see supporting information for calculation details). In all three single-layer films, the p-RSoXR-fitted δ -birefringence values at 283.9 eV and 284.7 eV align with a NEXAFS-calculated curve to within 5°, providing reassuring self-consistency, particularly as the relationship of δ -birefringence to γ is very different between these two energies. The 285.7 eV p-RSoXR data shows the same change in sign as the NEXAFS-calculated curves, providing further self-consistency on the direction of orientation; however, the magnitude of the δ -birefringence values at 285.7 eV are inconsistent with the 283.9 eV and 284.7 eV data. We attribute this discrepancy to a lower sensitivity to orientation at 285.7 eV (i.e., large changes in tilt result in smaller changes in δ -birefringence), as well as potential error in the fitted δ -values due to the coupling of the fitted δ and β values when β/δ becomes large⁴⁸. With this in mind, we interpret the bulk molecular tilt in the single-layer posaconazole films as the midpoint between the values from the 283.9 eV and 284.7 eV fit data and assume an uncertainty of $\gamma = +/-2.5^{\circ}$.

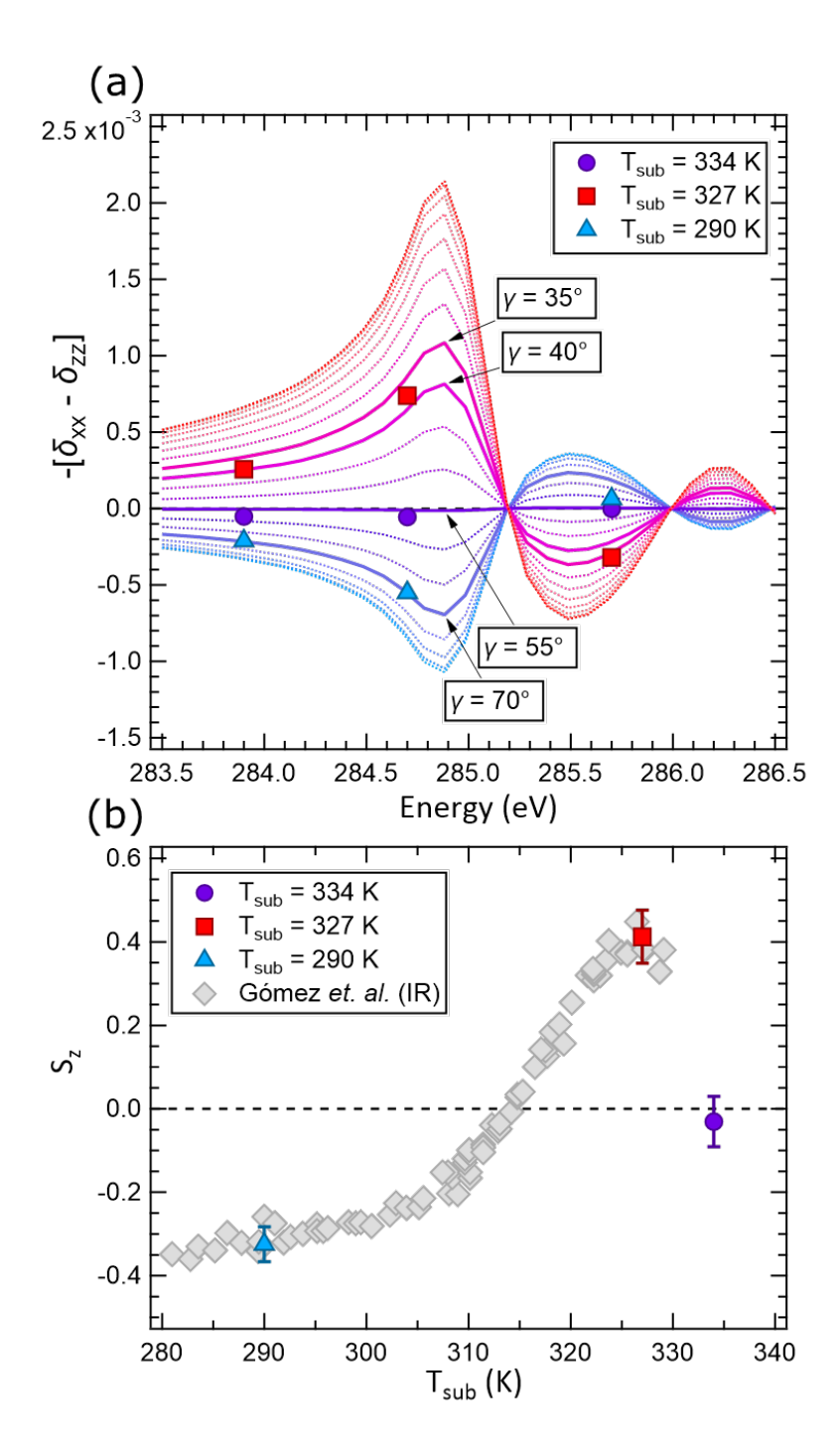


Figure 7: (a) Determination of molecular tilt γ from p-RSoXR analysis. The symbols correspond to the bulk δ-birefringence values extracted from fitting the p-RSoXR data of the isotropic (purple circles), horizontal (blue triangles), and vertical (red squares) posaconazole single-layer films. The curves represent isoclines of molecular tilt in 5° γ increments. The labeled curves, representing molecular tilts near the p-RSoXR fit values, are solid to guide the eye. (b) Comparison of the p-RSoXR-derived order parameter values (colored markers) with IR-derived results from ref 18 (grey diamonds). The error bars on the p-RSoXR-derived values correspond to +/- 2.5° in γ .

To test the accuracy of the molecular tilt values extracted from p-RSoXR, we calculate the orientational order parameter¹⁸, S_z , using Equation 2:

$$S_z = \frac{1}{2}(3 < \cos^2 \gamma > -1) \tag{2}$$

where \Leftrightarrow indicates the average over the orientation distribution function. In Figure 7b, we plot the p-RSoXR-derived S_z -values from the bulk along with the values reported by Gómez et al, which were determined using infrared (IR) spectroscopy¹⁸. We see excellent agreement between the two data sets. Interestingly, although the resonant interactions are vastly different between the two techniques, the tilt angle used to calculate S_z in both cases is related to the orientation of the core phenyl groups: we define γ based on the π^* plane from the core phenyl groups (Figure 2) in this work, and in the work of Gómez et al, the tilt angle was based on the in-plane bending of the C–H bonds of the core phenyl groups. Thus, although soft X-ray interaction physics are different than those of the IR probe, we can unambiguously quantify the same molecular tilt. Furthermore, the orders of magnitude shorter wavelength and reflectivity geometry of p-RSoXR allows us to achieve nanometer-scale orientation depth resolution.

The analysis of p-RSoXR data from the posaconazole single-layer films in Figure 4 through Figure 7 clearly demonstrates that the technique is sensitive to both bulk and surface orientation, and that combining information from NEXAFS and p-RSoXR can yield quantitative molecular tilt values for the bulk layer. At present, we only describe the surface layer orientation qualitatively: we can describe the tilt direction (horizontal or vertical) and if it is more or less oriented than the bulk tilt of that sample. Despite this remaining ambiguity, quantitative spatial correlations to simulated interface structures are nevertheless enabled by p-RSoXR, providing insight beyond bulk versus surface orientation studies. Depth profiles can also be valuable when interpreting the surface orientation from variable incident-angle NEXAFS. For example, if the oriented layer is

only \approx (1 to 2) nm, as it is in most of our films, and the effective electron mean free path of the NEXAFS PEY is \approx 1.5 nm, as it was at our PEY collection conditions (see Methods),⁴⁹ the tilt extracted from NEXAFS would be skewed toward the bulk value, as \approx 36 % NEXAFS signal would originate from molecules deeper than 1.5 nm.

Analyzing orientation in multilayer stacks

The power of p-RSoXR to measure orientation depth profiles extends beyond our results for single-layer films. Functional nanostructured thin films are rarely used as single layers; multilayer stacks are much more common. Multilayer stacks evoke additional structural questions related to the extent of intermixing between vertically adjacent layers. Previous study has explored the use of sequentially deposited multilayer stacks in stable glasses to characterize diffusion. ⁵⁰ Intermixing between layers of hydrogenated and deuterated versions of the same molecule were studied by NR, with results that provided early evidence that enhanced mobility within a few nanometers of the free surface was a key criterion for the formation of oriented stable glasses. ⁵⁰ We now apply the p-RSoXR technique to study an *orientationally* distinct bilayer stack.

We created the bilayer stack by sequential deposition of posaconazole, first at $T_{sub} = 327$ K, and then at $T_{sub} = 290$ K. The first deposition is expected to produce vertically oriented posaconazole, and the second deposition is expected to produce horizontally oriented posaconazole. We note that the temperature of the substrate during the second deposition is lower than that of the first deposition, so the bottom layer orientation should not be affected by the sequential thermal processing. In Figure 8 we show the resonant (284.7 eV) data, best-fit profiles, and corresponding orientation depth profile of this bilayer sample. Because the chemical composition within the two layers of the film are identical, the non-resonant data is well fit using an isotropic single layer

model (supporting information, Figure S21). However, the resonant reflectivity data shown in Figure 8a clearly indicate the presence of a more complex structure. Both polarizations show modulations in the reflected intensity at approximately every other fringe, with the modulation being particularly prominent in the p-pol data. This is a classic signature of bilayer reflectivity where both layers have similar film thickness. We emphasize that this behavior is due solely to changes in the refractive index induced by orientation; the top layer and bottom layer are chemically identical and were indistinguishable in the non-resonant (250 eV) p-RSoXR data. The presence of bilayer fringe modulations indicates that we are sensitive to the structure (broadness/roughness) of the internal orientation interface, which to our knowledge has never been measured before. We can extract the characteristics of this buried interface by fitting the p-RSoXR data using the same methodology developed for the single-layer films. The best fit required three layers to represent the posaconazole film: two ≈ 20 nm bulk layers and a ≈ 2.5 nm surface layer (see supporting information Table S8). The δ -birefringence values determined for the two bulk layers (Figure 8b) are in near quantitative agreement with the values determined for the singlelayer films deposited at each of the employed deposition conditions (Figure 5), proving that the bulk orientation of the bottom layer is not disturbed or otherwise altered by the deposition of the top layer, and that the vertical bottom layer does not orientationally 'template' or otherwise affect the orientation of the horizontal top layer. Also, the diffraction feature at high-q values caused by the smectic-like order of the vertical layer is once again observed, indicating that the translational ordering is also not affected by the sequential deposition.

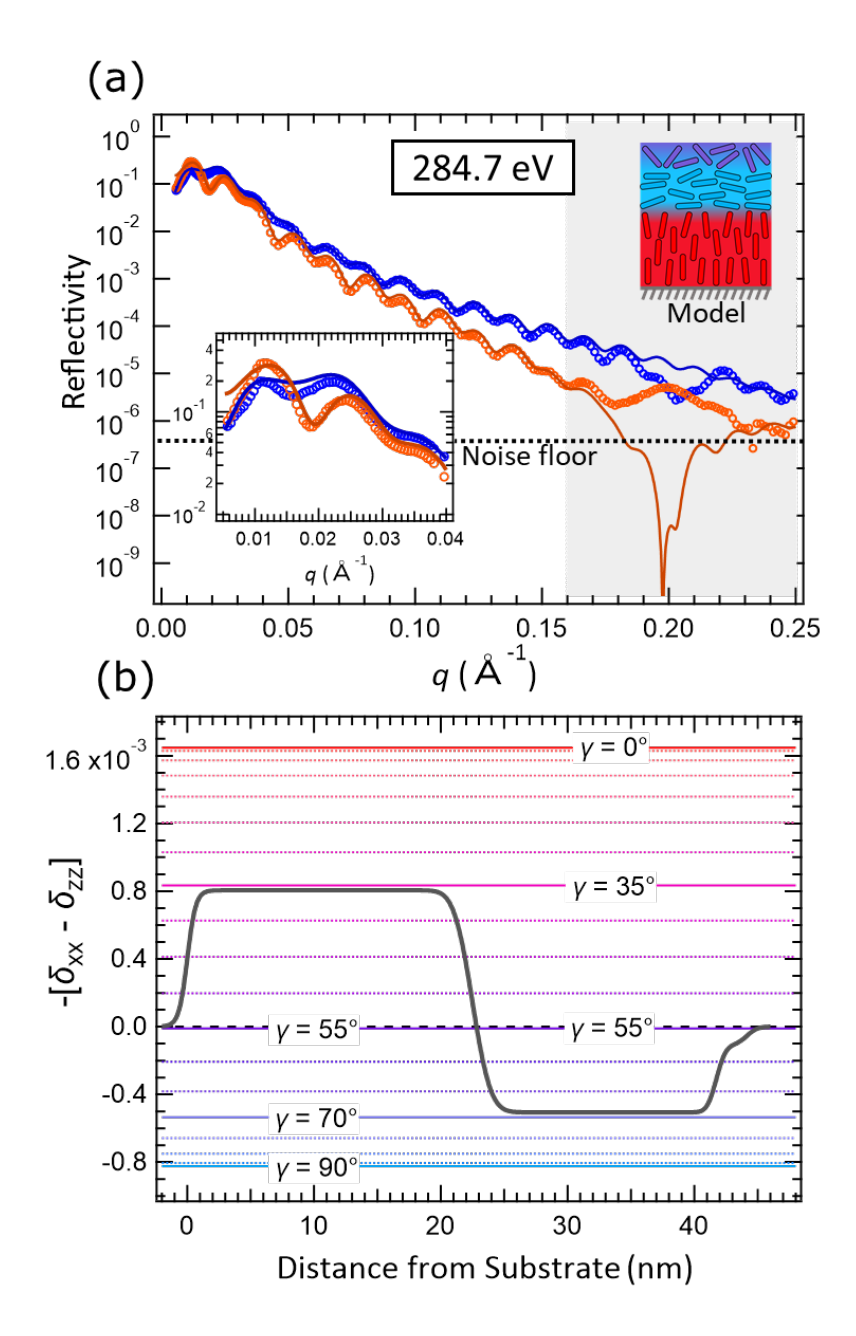


Figure 8: (a) p-RSoXR data collected from the orientation-bilayer posaconazole film using 284.7 eV X-rays. Blue circles and curves correspond to s-pol data and fits, respectively, and the orange circles and curves correspond to the p-pol data and fits. The s- and p-polarized data were fit simultaneously using three distinct layers and adjusting the layer thicknesses, their uniaxial dielectric tensors, and their interfacial width to model the posaconazole film. The inset highlights the low-q portion of the p-RSoXR data. (b) depth profile of the δ-birefringence values extracted from the fitted p-RSoXR data in (a). The colored horizontal lines indicate the expected δ-birefringence values for different γ values in 5° increments (as shown in Figure 7) at 284.7 eV.

Even though the bulk layer orientations appear unaffected by the formation of the bilayer stack, new behavior may be occurring at the buried interface. For our fitting process, we observe that it

is not necessary to include a thin, highly vertically oriented surface layer atop the vertical bottom layer in the bilayer stack, as one might expect from the single-layer film results (Figure 5f). Instead, we can model interface as a smooth transition in orientation, with an interfacial broadness of ≈ 2.8 nm, somewhat larger than the free surface broadness (roughness) of ≈ 1.7 nm. We speculate that during the deposition of the top layer, the surface layer of the bottom film may reorient to adopt a tilt more like the bulk of the vertical film, or that it may adopt an orientation that is transitional between the bottom and the top layer. Local rearrangement of the surface layer of the bottom film during top layer deposition would be consistent with NR observations of enhanced mobility, with the p-RSoXR results providing added insight into the orientational consequences of mixing in these mobile layers. In principle, by selecting appropriate measurement energies, p-RSoXR could be used to characterize both chemical composition and molecular orientation at the buried interfaces of multilayer stack films, which could provide unprecedented insight to the interfacial properties of multilayer film architectures, such as those used in OLED devices.

In addition to probing molecular orientation at the interface between bulk layers of a multilayer stack, p-RSoXR shows potential for being able to extract *submolecular* orientation details from smectic-like layered phases. To achieve even qualitative agreement with the high-q data shown in Figure 5c, our multi-layer model employed in the supporting information (Figure S19) required that the alternating layers have different levels of δ -birefringence, i.e., the diffraction effects in Figure 5c could not be reproduced by simple density fluctuations due to the regular packing of posaconazole molecules. The high-q behavior seen in Figure 5c and Figure 8a therefore requires the presence of an *orientational Bragg structure* in the smectic-like layering of the vertical posaconazole film. Because the δ and δ -birefringence values at 284.7 eV are affected by the 1s \rightarrow π^* transitions from multiple different carbon centers (see **Figure 1a**), we speculate that this

orientational Bragg structure is formed by alternating regions composed of the highly verticallyoriented rod-like core of posaconazole and the less oriented "floppy" end groups. If this capability to probe submolecular orientation proves general, it would enable previously inaccessible insights into the nanostructure of organic thin films.

Conclusions

Our framework for p-RSoXR measurements, where insights from variable incident-angle NEXAFS inform the quantitative interpretation of p-RSoXR-fitted δ -birefringence values, has revealed unprecedented details about molecular orientation in posaconazole glass films. New aspects to the nanostructure of this fascinating system are revealed, including the thickness of a highly oriented surface layer, orientational fluctuations within smectic-like ordered structures, and possible reorientation of highly mobile molecules at the buried interface of a bilayer stack. The capabilities of p-RSoXS enable several new avenues for studying stable glasses in the future, such as the possibility of bilayer thermal mixing experiments with orientation (rather than deuteration) contrast, or the exploration of vertical depth profiles of the extent of smectic-like order, to reveal its origins. This new measurement tool with high vertical resolution and a sensitivity to both composition and bond- or moiety-level orientation holds promise for great impact on the understanding of organic thin films that exhibit orientational or compositional heterogeneity, such as self-assembled materials, materials for energy storage, and organic electronics materials.

Acknowledgements

Work at the University of Wisconsin-Madison was supported by the National Science Foundation (NSF) through the University of Wisconsin Materials Research Science and Engineering Center (Grant DMR-1720415). J.L.T. acknowledges support from the National Research Council Research Associateship Program. p-RSoXR measurements were performed at beamline 11.0.1.2

of the Advanced Light Source, a U.S. Department of Energy (DOE) Office of Science User Facility under contract no. DE-AC02-05CH11231. We thank Cheng Wang for his assistance with operating beamline 11.0.1.2. We also acknowledge Elettra Sincrotrone Trieste for providing access to its synchrotron radiation facilities and we thank Luca Pasquali and Angelo Giglia for assistance in using the BEAR beamline to perform preliminary p-RSoXR experiments. We thank Tyler Martin for his assistance in developing the data reduction code for the beamline 11.0.1.2 data. J.L.T also thanks Edith Han for her support throughout the project. Certain commercial equipment, instruments, or materials (or suppliers, software, etc.) are identified in this paper to foster understanding. Such identification does not imply recommendation or endorsement by the National Institute of Standards and Technology, nor does it imply that the materials or equipment identified are necessarily the best available for the purpose.

Supporting Information Available: Description and results from the (1) VASE and (2) NEXAFS analysis of the single-layer posaconazole films, as well as (3) additional p-RSoXR data and analysis from all of the posaconazole films. This material is available free of charge via the Internet at http://pubs.acs.org.

References

- (1) Anastasiadis, S. H.; Russell, T. P.; Satija, S. K.; Majkrzak, C. F. The Morphology of Symmetric Diblock Copolymers as Revealed by Neutron Reflectivity. *J. Chem. Phys.* **1990**, 92 (9), 5677–5691. https://doi.org/10.1063/1.458499.
- (2) Sunday, D. F.; Chang, A. B.; Liman, C. D.; Gann, E.; Delongchamp, D. M.; Thomsen, L.; Matsen, M. W.; Grubbs, R. H.; Soles, C. L. Self-Assembly of ABC Bottlebrush Triblock Terpolymers with Evidence for Looped Backbone Conformations. *Macromolecules* **2018**, 51 (18), 7178–7185. https://doi.org/10.1021/acs.macromol.8b01370.
- (3) Campoy-Quiles, M.; Ferenczi, T.; Agostinelli, T.; Etchegoin, P. G.; Kim, Y.; Anthopoulos, T. D.; Stavrinou, P. N.; Bradley, D. D. C.; Nelson, J. Morphology Evolution via Self-Organization and Lateral and Vertical Diffusion in Polymer:Fullerene Solar Cell Blends. *Nat. Mater.* **2008**, *7* (2), 158–164. https://doi.org/10.1038/nmat2102.
- (4) Germack, D. S.; Chan, C. K.; Kline, R. J.; Fischer, D. A.; Gundlach, D. J.; Toney, M. F.; Richter, L. J.; DeLongchamp, D. M. Interfacial Segregation in Polymer/Fullerene Blend Films for Photovoltaic Devices. *Macromolecules* **2010**, *43* (8), 3828–3836. https://doi.org/10.1021/ma100027b.

- (5) Treat, N. D.; Brady, M. A.; Smith, G.; Toney, M. F.; Kramer, E. J.; Hawker, C. J.; Chabinyc, M. L. Interdiffusion of PCBM and P3HT Reveals Miscibility in a Photovoltaically Active Blend. *Adv. Energy Mater.* 2011, 1 (1), 82–89. https://doi.org/10.1002/aenm.201000023.
- (6) Gann, E.; Caironi, M.; Noh, Y. Y.; Kim, Y. H.; McNeill, C. R. Diffractive X-Ray Waveguiding Reveals Orthogonal Crystalline Stratification in Conjugated Polymer Thin Films. *Macromolecules* **2018**, *51* (8), 2979–2987. https://doi.org/10.1021/acs.macromol.8b00168.
- (7) Wu, D.; Kaplan, M.; Ro, H. W.; Engmann, S.; Fischer, D. A.; DeLongchamp, D. M.; Richter, L. J.; Gann, E.; Thomsen, L.; McNeill, C. R.; others. Blade Coating Aligned, High-Performance, Semiconducting-Polymer Transistors. *Chem. Mater.* **2018**, *30* (6), 1924–1936.
- (8) Mezger, M.; Schröder, H.; Reichert, H.; Schramm, S.; Okasinski, J. S.; Schöder, S.; Honkimäki, V.; Deutsch, M.; Ocko, B. M.; Ralston, J.; Rohwerder, M.; Stratmann, M.; Dosch, H. Molecular Layering of Fluorinated Ionic Liquids at a Charged Sapphire (0001) Surface. *Science* **2008**, *322* (5900), 424–428. https://doi.org/10.1126/science.1164502.
- (9) Gilbert, J. B.; Luo, M.; Shelton, C. K.; Rubner, M. F.; Cohen, R. E.; Epps, T. H. Determination of Lithium-Ion Distributions in Nanostructured Block Polymer Electrolyte Thin Films by X-Ray Photoelectron Spectroscopy Depth Profiling. *ACS Nano* **2015**, *9* (1), 512–520. https://doi.org/10.1021/nn505744r.
- (10) Kolesov, V. A.; Fuentes-Hernandez, C.; Chou, W.-F.; Aizawa, N.; Larrain, F. A.; Wang, M.; Perrotta, A.; Choi, S.; Graham, S.; Bazan, G. C.; Nguyen, T.-Q.; Marder, S. R.; Kippelen, B. Solution-Based Electrical Doping of Semiconducting Polymer Films over a Limited Depth. *Nat. Mater.* **2017**, *16* (4), 474–480. https://doi.org/10.1038/nmat4818.
- (11) Armas-Pérez, J. C.; Li, X.; Martínez-González, J. A.; Smith, C.; Hernández-Ortiz, J. P.; Nealey, P. F.; de Pablo, J. J. Sharp Morphological Transitions from Nanoscale Mixed-Anchoring Patterns in Confined Nematic Liquid Crystals. *Langmuir* **2017**, *33* (43), 12516–12524. https://doi.org/10.1021/acs.langmuir.7b02522.
- (12) Heinrich, F.; Lösche, M. Zooming in on Disordered Systems: Neutron Reflection Studies of Proteins Associated with Fluid Membranes. *Biochim. Biophys. Acta BBA Biomembr.* **2014**, *1838* (9), 2341–2349. https://doi.org/10.1016/j.bbamem.2014.03.007.
- (13) Lin, E. K.; Soles, C. L.; Goldfarb, D. L.; Trinque, B. C.; Burns, S. D.; Jones, R. L.; Lenhart, J. L.; Angelopoulos, M.; Willson, C. G.; Satija, S. K.; Wu, W. Direct Measurement of the Reaction Front in Chemically Amplified Photoresists. *Science* **2002**, *297* (5580), 372–375. https://doi.org/10.1126/science.1072092.
- (14) Walters, D. M.; Antony, L.; de Pablo, J. J.; Ediger, M. D. Influence of Molecular Shape on the Thermal Stability and Molecular Orientation of Vapor-Deposited Organic Semiconductors. *J. Phys. Chem. Lett.* **2017**, 8 (14), 3380–3386. https://doi.org/10.1021/acs.jpclett.7b01097.
- (15) Lyubimov, I.; Antony, L.; Walters, D. M.; Rodney, D.; Ediger, M. D.; De Pablo, J. J. Orientational Anisotropy in Simulated Vapor-Deposited Molecular Glasses. *J. Chem. Phys.* **2015**, *143* (9). https://doi.org/10.1063/1.4928523.
- (16) Yokoyama, D. Molecular Orientation in Small-Molecule Organic Light-Emitting Diodes. *J. Mater. Chem.* **2011**, *21* (48), 19187. https://doi.org/10.1039/c1jm13417e.
- (17) Ediger, M. D.; De Pablo, J.; Yu, L. Anisotropic Vapor-Deposited Glasses: Hybrid Organic Solids. *Acc. Chem. Res.* **2019**, *52* (2), 407–414. https://doi.org/10.1021/acs.accounts.8b00513.

- (18) Gómez, J.; Gujral, A.; Huang, C.; Bishop, C.; Yu, L.; Ediger, M. D. Nematic-like Stable Glasses without Equilibrium Liquid Crystal Phases. *J. Chem. Phys.* **2017**, *146* (5), 054503. https://doi.org/10.1063/1.4974829.
- (19) Dalal, S. S.; Walters, D. M.; Lyubimov, I.; de Pablo, J. J.; Ediger, M. D. Tunable Molecular Orientation and Elevated Thermal Stability of Vapor-Deposited Organic Semiconductors. *Proc. Natl. Acad. Sci.* **2015**, *112* (14), 4227–4232. https://doi.org/10.1073/pnas.1421042112.
- (20) Bishop, C.; Thelen, J. L.; Gann, E.; Toney, M. F.; Yu, L.; DeLongchamp, D. M.; Ediger, M. D. Vapor Deposition of a Nonmesogen Prepares Highly Structured Organic Glasses. *Proc. Natl. Acad. Sci.* 2019, 201908445. https://doi.org/10.1073/pnas.1908445116.
- (21) Ràfols-Ribé, J.; Will, P.-A.; Hänisch, C.; Gonzalez-Silveira, M.; Lenk, S.; Rodríguez-Viejo, J.; Reineke, S. High-Performance Organic Light-Emitting Diodes Comprising Ultrastable Glass Layers. *Sci. Adv.* **2018**, *4* (5), eaar8332. https://doi.org/10.1126/sciadv.aar8332.
- (22) Snyder, C. R.; DeLongchamp, D. M. Glassy Phases in Organic Semiconductors. *Curr. Opin. Solid State Mater. Sci.* **2018**.
- (23) Hamann-Borrero, J. E.; Macke, S.; Gray, B.; Kareev, M.; Schierle, E.; Partzsch, S.; Zwiebler, M.; Treske, U.; Koitzsch, A.; Büchner, B.; Freeland, J. W.; Chakhalian, J.; Geck, J. Site-Selective Spectroscopy with Depth Resolution Using Resonant x-Ray Reflectometry. *Sci. Rep.* **2017**, *7* (1), 1–11. https://doi.org/10.1038/s41598-017-12642-7.
- (24) Benckiser, E.; Haverkort, M. W.; Brück, S.; Goering, E.; Macke, S.; Frañó, A.; Yang, X.; Andersen, O. K.; Cristiani, G.; Habermeier, H.-U.; Boris, A. V.; Zegkinoglou, I.; Wochner, P.; Kim, H.-J.; Hinkov, V.; Keimer, B. Orbital Reflectometry of Oxide Heterostructures. *Nat. Mater.* **2011**, *10* (3), 189–193. https://doi.org/10.1038/nmat2958.
- (25) Macke, S.; Goering, E. Magnetic Reflectometry of Heterostructures. *J. Phys. Condens. Matter* **2014**, *26* (36), 363201. https://doi.org/10.1088/0953-8984/26/36/363201.
- (26) Wang, C.; Araki, T.; Ade, H. Soft X-Ray Resonant Reflectivity of Low-Z Material Thin Films. *Appl. Phys. Lett.* **2005**, 87 (21), 214109. https://doi.org/10.1063/1.2136353.
- (27) Wang, C.; Araki, T.; Watts, B.; Harton, S.; Koga, T.; Basu, S.; Ade, H. Resonant Soft X-Ray Reflectivity of Organic Thin Films. *J. Vac. Sci. Technol. Vac. Surf. Films* **2007**, *25* (3), 575–586. https://doi.org/10.1116/1.2731352.
- (28) Yan, H.; Wang, C.; Garcia, A.; Swaraj, S.; Gu, Z.; McNeill, C. R.; Schuettfort, T.; Sohn, K. E.; Kramer, E. J.; Bazan, G. C.; Nguyen, T.-Q.; Ade, H. Interfaces in Organic Devices Studied with Resonant Soft X-Ray Reflectivity. *J. Appl. Phys.* **2011**, *110* (10), 102220-102220-102229. https://doi.org/doi:10.1063/1.3661991.
- (29) Sunday, D. F.; Kline, R. J. Reducing Block Copolymer Interfacial Widths through Polymer Additives. *Macromolecules* **2015**, *48* (3), 679–686. https://doi.org/10.1021/ma502015u.
- (30) Mezger, M.; Jérôme, B.; Kortright, J. B.; Valvidares, M.; Gullikson, E. M.; Giglia, A.; Mahne, N.; Nannarone, S. Molecular Orientation in Soft Matter Thin Films Studied by Resonant Soft X-Ray Reflectivity. *Phys. Rev. B* **2011**, *83* (15), 155406. https://doi.org/10.1103/PhysRevB.83.155406.
- (31) Capelli, R.; Mahne, N.; Koshmak, K.; Giglia, A.; Doyle, B. P.; Mukherjee, S.; Nannarone, S.; Pasquali, L. Quantitative Resonant Soft X-Ray Reflectivity of Ultrathin Anisotropic Organic Layers: Simulation and Experiment of PTCDA on Au. *J. Chem. Phys.* **2016**, *145* (2). https://doi.org/10.1063/1.4956452.
- (32) Pasquali, L.; Mukherjee, S.; Terzi, F.; Giglia, A.; Mahne, N.; Koshmak, K.; Esaulov, V.; Toccafondi, C.; Canepa, M.; Nannarone, S. Structural and Electronic Properties of

- Anisotropic Ultrathin Organic Films from Dichroic Resonant Soft X-Ray Reflectivity. *Phys. Rev. B* **2014**, *89* (4), 045401. https://doi.org/10.1103/PhysRevB.89.045401.
- (33) Shard, A. G.; Brewer, P. J.; Green, F. M.; Gilmore, I. S. Measurement of Sputtering Yields and Damage in C60 SIMS Depth Profiling of Model Organic Materials. *Surf. Interface Anal.* **2007**, *39* (4), 294–298. https://doi.org/10.1002/sia.2525.
- (34) Chen, Y.; Yu, B.; Wang, W.; Hsu, M.; Lin, W.; Lin, Y.; Jou, J.; Shyue, J. X-Ray Photoelectron Spectrometry Depth Profiling of Organic Thin Films Using C 60 Sputtering. **2008**, 80 (2), 501–505. https://doi.org/10.1021/ac701899a.
- (35) Russell, T. P. X-Ray and Neutron Reflectivity for the Investigation of Polymers. *Mater. Sci. Rep.* **1990**, *5* (4), 171–271. https://doi.org/10.1016/S0920-2307(05)80002-7.
- (36) Campoy-Quiles, M.; Alonso, M. I.; Bradley, D. D. C.; Richter, L. J. Advanced Ellipsometric Characterization of Conjugated Polymer Films. *Adv. Funct. Mater.* **2014**, *24* (15), 2116–2134. https://doi.org/10.1002/adfm.201303060.
- (37) Attwood, D. *Soft X-Rays and Extreme Ultraviolet Radiation*; Cambridge University Press: Cambridge, 1999. https://doi.org/10.1017/CBO9781139164429.
- (38) DeLongchamp, D. M.; Kline, R. J.; Lin, E. K.; Fischer, D. A.; Richter, L. J.; Lucas, L. A.; Heeney, M.; McCulloch, I.; Northrup, J. E. High Carrier Mobility Polythiophene Thin Films: Structure Determination by Experiment and Theory. *Adv. Mater.* **2007**, *19* (6), 833–837. https://doi.org/10.1002/adma.200602651.
- (39) Cowie, B. C. C.; Tadich, A.; Thomsen, L.; Garrett, R.; Gentle, I.; Nugent, K.; Wilkins, S. The Current Performance of the Wide Range (90–2500 EV) Soft X-Ray Beamline at the Australian Synchrotron; 2010; pp 307–310. https://doi.org/10.1063/1.3463197.
- (40) Gann, E.; McNeill, C. R.; Tadich, A.; Cowie, B. C. C.; Thomsen, L. Quick AS NEXAFS Tool (QANT): A Program for NEXAFS Loading and Analysis Developed at the Australian Synchrotron. *J. Synchrotron Radiat.* **2016**, *23* (1), 374–380. https://doi.org/10.1107/S1600577515018688.
- (41) Wang, C.; Hexemer, A.; Nasiatka, J.; Chan, E. R.; Young, A. T.; Padmore, H. A.; Schlotter, W. F.; Lüning, J.; Swaraj, S.; Watts, B.; Gann, E.; Yan, H.; Ade, H. Resonant Soft X-Ray Scattering of Polymers with a 2D Detector: Initial Results and System Developments at the Advanced Light Source. *IOP Conf. Ser. Mater. Sci. Eng.* **2010**, *14*, 012016. https://doi.org/10.1088/1757-899x/14/1/012016.
- (42) Collins, B. a; Cochran, J. E.; Yan, H.; Gann, E.; Hub, C.; Fink, R.; Wang, C.; Schuettfort, T.; McNeill, C. R.; Chabinyc, M. L.; Ade, H. Polarized X-Ray Scattering Reveals Non-Crystalline Orientational Ordering in Organic Films. *Nat. Mater.* **2012**, *11* (6), 536–543. https://doi.org/10.1038/nmat3310.
- (43) Nannarone, S.; Borgatti, F.; DeLuisa, A.; Doyle, B. P.; Gazzadi, G. C.; Giglia, A.; Finetti, P.; Mahne, N.; Pasquali, L.; Pedio, M.; Selvaggi, G.; Naletto, G.; Pelizzo, M. G.; Tondello, G. The BEAR Beamline at Elettra. *AIP Conf. Proc.* **2004**, *705* (1), 450–453. https://doi.org/10.1063/1.1757831.
- (44) Macke, S.; Goering, E. Magnetic Reflectometry of Heterostructures. *J. Phys. Condens. Matter* **2014**, *26* (36), 363201. https://doi.org/10.1088/0953-8984/26/36/363201.
- (45) Zwiebler, M.; Hamann-Borrero, J. E.; Vafaee, M.; Komissinskiy, P.; Macke, S.; Sutarto, R.; He, F.; Büchner, B.; Sawatzky, G. A.; Alff, L.; Geck, J. Electronic Depth Profiles with Atomic Layer Resolution from Resonant Soft X-Ray Reflectivity. *New J. Phys.* **2015**, *17* (8), 083046. https://doi.org/10.1088/1367-2630/17/8/083046.
- (46) Stöhr, J. NEXAFS Spectroscopy, Corrected edition.; Springer: Berlin; New York, 2003.

- (47) Adrjanowicz, K.; Kaminski, K.; Włodarczyk, P.; Grzybowska, K.; Tarnacka, M.; Zakowiecki, D.; Garbacz, G.; Paluch, M.; Jurga, S. Molecular Dynamics of the Supercooled Pharmaceutical Agent Posaconazole Studied via Differential Scanning Calorimetry and Dielectric and Mechanical Spectroscopies. *Mol. Pharm.* **2013**, *10* (10), 3934–3945. https://doi.org/10.1021/mp4003915.
- (48) Soufli, R.; Gullikson, E. M. Reflectance Measurements on Clean Surfaces for the Determination of Optical Constants of Silicon in the Extreme Ultraviolet–Soft-x-Ray Region. *Appl. Opt.* **1997**, *36* (22), 5499–5507. https://doi.org/10.1364/AO.36.005499.
- (49) Zharnikov, M.; Frey, S.; Heister, K.; Grunze, M. An Extension of the Mean Free Path Approach to X-Ray Absorption Spectroscopy. *J. Electron Spectrosc. Relat. Phenom.* **2002**, 124 (1), 15–24. https://doi.org/10.1016/S0368-2048(02)00004-X.
- (50) Swallen, S. F.; Kearns, K. L.; Mapes, M. K.; Kim, Y. S.; McMahon, R. J.; Ediger, M. D.; Wu, T.; Yu, L.; Satija, S. Organic Glasses with Exceptional Thermodynamic and Kinetic Stability. *Science* **2007**, *315* (5810), 353–356. https://doi.org/10.1126/science.1135795.

For Table of Contents Use Only

